frontiers | Frontiers in Cell and Developmental Biology

TYPE Original Research
PUBLISHED 01 November 2022
DOI 10.3389/fcell.2022.1008542

OPEN ACCESS

EDITED BY
Omar Skalli,
University of Memphis, United States

REVIEWED BY
David F. Meaney,
University of Pennsylvania, United States
Rui Liu,
Yangzhou University, China

*CORRESPONDENCE
Natasha T. Snider,
ntsnider@med.unc.edu

SPECIALTY SECTION
This article was submitted to Signaling, a section of the journal Frontiers in Cell and Developmental Biology

RECEIVED 31 July 2022
ACCEPTED 04 October 2022
PUBLISHED 01 November 2022

CITATION
Phillips CL, Fu D, Herring LE, Armao D and Snider NT (2022), Calpain-mediated proteolysis of vimentin filaments is augmented in giant axonal neuropathy fibroblasts exposed to hypotonic stress. *Front. Cell Dev. Biol.* 10:1008542. doi: 10.3389/fcell.2022.1008542

Calpain-mediated proteolysis of vimentin filaments is augmented in giant axonal neuropathy fibroblasts exposed to hypotonic stress

Cassandra L. Phillips[1], Dong Fu[2], Laura E. Herring[3], Diane Armao[4,5] and Natasha T. Snider[1]*

[1]Department of Cell Biology and Physiology, University of North Carolina at Chapel Hill, Chapel Hill, NC, United States, [2]Division of Pharmacotherapy and Experimental Therapeutics, UNC Eshelman School of Pharmacy, University of North Carolina at Chapel Hill, Chapel Hill, NC, United States, [3]UNC Proteomics Core Facility, Department of Pharmacology, University of North Carolina at Chapel Hill, Chapel Hill, NC, United States, [4]Department of Pathology and Laboratory Medicine, University of North Carolina at Chapel Hill, Chapel Hill, NC, United States, [5]Department of Radiology, University of North Carolina at Chapel Hill, Chapel Hill, NC, United States

Giant Axonal Neuropathy (GAN) is a pediatric neurodegenerative disease caused by loss-of-function mutations in the E3 ubiquitin ligase adaptor gigaxonin, which is encoded by the *KLHL16* gene. Gigaxonin regulates the degradation of multiple intermediate filament (IF) proteins, including neurofilaments, GFAP, and vimentin, which aggregate in GAN patient cells. Understanding how IFs and their aggregates are processed under stress can reveal new GAN disease mechanisms and potential targets for therapy. Here we tested the hypothesis that hypotonic stress-induced vimentin proteolysis is impaired in GAN. In both GAN and control fibroblasts exposed to hypotonic stress, we observed time-dependent vimentin cleavage that resulted in two prominent ~40–45 kDa fragments. However, vimentin proteolysis occurred more rapidly and extensively in GAN cells compared to unaffected controls as both fragments were generated earlier and at 4-6-fold higher levels. To test enzymatic involvement, we determined the expression levels and localization of the calcium-sensitive calpain proteases-1 and -2 and their endogenous inhibitor calpastatin. While the latter was not affected, the expression of both calpains was 2-fold higher in GAN cells compared to control cells. Moreover, pharmacologic inhibition of calpains with MDL-28170 or MG-132 attenuated vimentin cleavage. Imaging analysis revealed striking colocalization between large perinuclear vimentin aggregates and calpain-2 in GAN fibroblasts. This colocalization was dramatically altered by hypotonic stress, where selective breakdown of filaments over aggregates occurred rapidly in GAN cells and coincided with calpain-2 cytoplasmic redistribution. Finally, mass spectrometry-based proteomics revealed that phosphorylation at Ser-412, located at the junction between the central "rod" domain and C-terminal "tail" domain on vimentin, is involved in this stress response. Over-expression studies using phospho-deficient and phospho-mimic mutants revealed that Ser-412 is important for filament organization, solubility

dynamics, and vimentin cleavage upon hypotonic stress exposure. Collectively, our work reveals that osmotic stress induces calpain- and proteasome-mediated vimentin degradation and IF network breakdown. These effects are significantly augmented in the presence of disease-causing *KLHL16* mutations that alter intermediate filament organization. While the specific roles of calpain-generated vimentin IF fragments in GAN cells remain to be defined, this proteolytic pathway is translationally-relevant to GAN because maintaining osmotic homeostasis is critical for nervous system function.

KEYWORDS

protease, fragments, protein aggregation, gigaxonin, post-translational modifications

Introduction

Intermediate filament (IF) proteins form filamentous networks that support cell structure and function (Lowery et al., 2015). Encoded by more than 70 individual genes in humans, IFs serve as organizers of the cytoplasmic space, scaffolds of interacting proteins within signaling networks, and mediators of stress responses (Etienne-Manneville, 2018). With respect to the latter, IF protein networks are known to be extensively remodeled in cells undergoing stress, which is critical for their many cytoprotective functions (Coulombe and Wong, 2004; Toivola et al., 2010). The remarkable plasticity of cytoplasmic IFs is highly dependent on various post-translational modifications (PTM), including phosphorylation, acetylation, sumoylation, and enzymatic proteolysis (Snider and Omary, 2014). Regulated cross talk between the various PTMs on IF proteins imparts a significant level of complexity to the system to ensure appropriate homeostatic and allostatic responses.

While IFs are critical for providing cells with stress resilience, chronic unresolved stress or genetic mutations can give rise to focal abnormal cytoplasmic IF accumulations (aggregates) in various cell types (Ku et al., 2007; Didonna and Opal, 2019; Viedma-Poyatos et al., 2020; Yang et al., 2022). The structural nature and precise roles of cell type-specific IF aggregates remain unclear. Yet, in the context of IF-associated human disease, gain of IF aggregates over time is accompanied by clinical decompensation and disease progression (Robertson et al., 2001; Xiao et al., 2008; Rakoski et al., 2011; Sosunov et al., 2017; Rainer et al., 2018; Kedia et al., 2019). This is particularly evident in the pediatric neurodegenerative disease Giant Axonal Neuropathy (GAN), which is caused by loss-of-function mutations in the gene *KLHL16* (also called *GAN*) (Johnson-Kerner et al., 2014). *KLHL16* encodes the protein gigaxonin (Bomont et al., 2000) - an adapter of an E3 ubiquitin-ligase complex that targets IF proteins for proteasomal degradation (Mahammad et al., 2013). In the absence of functional gigaxonin, multiple IF proteins, including desmin, neurofilaments, GFAP, and vimentin, accumulate in different cell types in GAN patients (Thomas et al., 1987; Mohri et al., 1998; Leung et al., 2007; Nalini et al., 2008). Pathologic diagnosis of GAN is based on dense bundles of IF accumulations causing focal, greatly enlarged, axonal swellings, or "giant axons," after which the disease was named (Asbury et al., 1972). GAN affects both the peripheral nervous system (PNS) and the central nervous system (CNS). The natural history of GAN is characterized by progressive motor and sensory loss, with patients being non-ambulatory by the second decade of life, and death usually during the third decade (Bharucha-Goebel et al., 2021). Therefore, new mechanistic insights into the genesis and dismantling of IF aggregates will advance the development of therapeutic targets for IF-associated diseases like GAN. Importantly, proteolytic pathways for IF degradation in GAN patient cells exposed to external stress have not been characterized.

In general, exposure to stress affects the IF network composition and organization, as well as IF solubility dynamics, which are significantly altered in cells with persistent IF aggregates (Dutour-Provenzano and Etienne-Manneville, 2021). Osmotic stress in particular is known to regulate IF solubility and network formation (Li et al., 2019). Recently, it was shown that brief hypotonic exposure caused rapid and reversible reorganization and breakdown of the vimentin IFs, and that this occurred prior to any significant alterations in the actin and microtubule cytoskeletal networks (Pan et al., 2019). Moreover, it is known that cells lacking vimentin are more susceptible to hypotonic stress, suggesting that rapid vimentin reorganization may be important in this cytoprotective response (Li et al., 2019). Proteolytic vimentin cleavage and vimentin IF network disassembly also play an active role during inflammatory programmed cell death (pyroptosis) (Davis et al., 2019), where the loss of filaments results in reduced mechanical resilience in response to external stressors, ultimately leading to cell rupture and the release of immunostimulatory cellular components. Given the importance of stress-dependent vimentin cleavage in different cellular responses, we tested the hypothesis that stress-induced vimentin proteolysis is impaired in GAN.

To that end, we exposed GAN patient-derived and unaffected control fibroblasts to hypotonic stress for brief periods and analyzed vimentin changes biochemically and by immunofluorescence imaging. Collectively, our results show

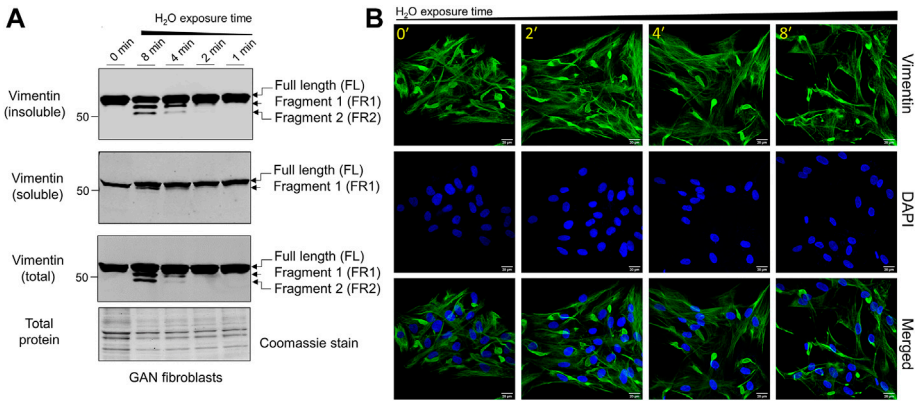

FIGURE 1
Hypotonic stress induces time-dependent cleavage and reorganization of vimentin IFs in GAN fibroblasts. **(A)** Immunoblotting of vimentin in reduced Triton X insoluble pellet fractions (top), Triton X soluble fractions (middle), and total cell lysates (bottom) from GAN fibroblasts (GAO1B) exposed to hypotonic stress conditions (sterile molecular grade H_2O) for 0–8 min. Only full length (FL) vimentin is present in the 0-min condition (lane 1), but a time-dependent, osmotic stress-induced increase in vimentin cleavage is observed starting in the 2-min condition (lane 4). The two vimentin fragments (FR1, FR2) produced are most abundant in the 8-min condition (lane 2). Coomassie stain was used as a control for total protein. **(B)** Immunofluorescence analysis of GAN fibroblasts (B16.64) stained with vimentin (green) and DAPI (blue) after exposure to water for 0–8 min; scale bar = 20 μm. Note the persistence of vimentin aggregates, but a reduction in vimentin filaments.

that hypotonic stress induces calpain- and proteasome-mediated vimentin degradation and IF network breakdown, and that there are regulatory phosphorylation sites located at the junction between the rod and C-terminal tail domains on vimentin that are involved in this IF stress response. Contrary to our hypothesis, vimentin breakdown occurred more rapidly and extensively in GAN cells compared to controls, raising the possibility that vimentin cleavage products may be involved in cellular dysfunction in GAN. While the specific roles of calpain-generated vimentin fragments in GAN remain to be defined, this proteolytic pathway is translationally-relevant to the disease pathogenesis of GAN because maintaining osmotic homeostasis is critically important for homeostasis and nervous system function (Bourque, 2008).

Results

Hypotonic stress promotes time-dependent cleavage and reorganization of vimentin IFs in GAN fibroblasts. Given the different organization of vimentin IFs in GAN fibroblasts, which is characterized by the presence of both cytoplasmic filaments and perinuclear ovoid bundles (Mahammad et al., 2013), we asked whether vimentin cleavage will occur in a similar fashion in GAN cells. To that end, we exposed GAN patient-derived fibroblasts to hypotonic stress using water exposure, as was done previously (Pan et al., 2019), for 0–8 min. Since osmotic stress is known to alter IF protein solubility, we compared vimentin in total cell lysates and Triton X detergent-insoluble and detergent-soluble fractions. As shown in Figure 1A, there was time-dependent vimentin cleavage in the GAN fibroblasts, resulting in two prominent fragments (FR1, FR2) detected by western blot in the total cell lysates and detergent-insoluble fractions, in addition to full length vimentin. Small amounts of cleaved vimentin (FR1) were also seen in the detergent-soluble fraction after 8 min of treatment (Figure 1A). The two cleaved products were most abundant in the 8-min exposure condition, indicating that prolonged exposure resulted in increased breakdown of vimentin and/or decreased downstream processing of the smaller fragments (Figure 1A). Disruption of vimentin IFs in GAN fibroblasts was also observed by immunofluorescence imaging, as longer exposure time to hypotonic stress resulted in the progressive reduction of cytoplasmic vimentin filaments, while perinuclear aggregates persisted across conditions (Figure 1B). These results indicated that vimentin IFs in GAN cells were sensitive to hypotonic stress, but the vimentin aggregates were more resistant to this treatment.

Hypotonic stress-induced vimentin cleavage is augmented in GAN compared to control fibroblasts. Next, we asked whether vimentin cleavage under hypotonic stress is altered in GAN compared to control (unaffected) fibroblasts. Direct comparison of cleaved vimentin products over time revealed the presence of vimentin fragments at earlier time points and at higher levels in the detergent-insoluble fractions of GAN cells compared to control cells (Figure 2A). In the GAN cells, both cleaved vimentin fragments can be observed in the 2-min condition and were highly abundant in the 8-min condition (Figure 2A). In the control cells, there was no evidence of vimentin cleavage until the 8-min condition, and the levels of the fragments were lower when normalized to full length vimentin (Figure 2B).

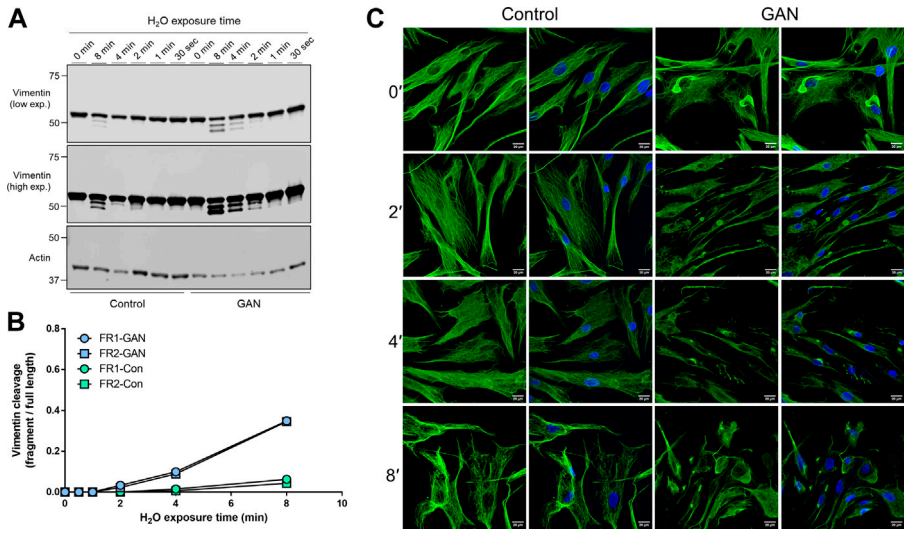

FIGURE 2
Hypotonic stress-induced vimentin cleavage is augmented in GAN compared to control fibroblasts. **(A)** Immunoblotting of vimentin (top and middle) and actin (bottom; loading control) in reduced Triton X insoluble pellet fractions from control (lanes 1–6) and GAN (GAO1B; lanes 7–12) fibroblasts exposed to hypotonic stress conditions (sterile molecular grade H_2O) for 0–8 min. Expression of the two vimentin fragments (FR1 and FR2) is increased in GAN patient cells compared to control cells. Low (top) and high (middle) exposure blots of the same membrane are shown for vimentin. **(B)** Densitometry quantification of vimentin fragment (FR) intensities relative to full length vimentin in control and GAN fibroblasts exposed to hypotonic stress for 0–8 min. Data points represent values from a single experiment and are representative of at least three independent experiments. **(C)** Immunofluorescence analysis of control 56.3 and GAN 56.1 fibroblasts stained with vimentin (green) and DAPI (blue) after exposure to water for 0–8 min; scale bar = 20 μm. Note significant breakdown of the vimentin filament network in the GAN cells at an earlier timepoint (2′) compared to the control cells (8′).

Immunofluorescence staining for vimentin corroborated the biochemical analysis, indicating that vimentin IFs in control fibroblasts were more resistant to reorganization and filament breakdown under hypotonic stress (Figure 2C). These data suggested that vimentin IFs in GAN fibroblasts were more sensitive to hypotonic stress-induced cleavage. This prompted us to determine if calpains, proteolytic enzymes that have been previously implicated in vimentin cleavage producing the same pattern of fragmentation (Nelson and Traub, 1983a; Dourdin et al., 1999), were involved in the vimentin processing observed in GAN cells.

Vimentin cleavage is blocked by inhibitors of the proteasome and calpains, which are elevated in GAN. Pre-treatment with the calpain inhibitor MDL-28170, followed by 8 min of water exposure reduced, but did not eliminate vimentin cleavage in the control and GAN cells (Figure 3A). However, the fragments were nearly undetectable in the presence of MG-132, which inhibits calpains and the proteasome (Figure 3A). MG-132 eliminated vimentin cleavage comparably in both control and GAN fibroblasts (Figure 3B), suggesting the involvement of similar proteolytic pathways. However, we detected significantly higher levels of calpain-1 and -2 in GAN cells compared to control cells, but no major differences in calpastatin, an endogenous inhibitor of calpain activity in cells (Figures 3B,D). The increased calpain expression correlated with increased cleavage of vimentin in GAN cells (Figure 3C). Therefore, increased calpain-1/2 expression may account, at least in part, for the increased vimentin cleavage in GAN cells exposed to hypotonic stress.

Calpain-2 colocalizes with perinuclear vimentin aggregates and undergoes cytoplasmic redistribution upon hypotonic stress exposure. In addition to the biochemical analyses, we investigated calpain localization *via* immunofluorescence imaging. Interestingly, the imaging analyses revealed prominent colocalization between large perinuclear vimentin aggregates and calpain-2 in the untreated GAN patient fibroblasts (Figure 4A). However, calpain-2 localization was dramatically altered following 4 min of hypotonic stress exposure (Figure 4B). In addition to vimentin network breakdown in response to stress, calpain-2 staining became more punctate and distributed throughout the cytoplasm, which was largely devoid of filaments (Figure 4B). This cytoplasmic redistribution of calpain-2 indicated a rapid and selective breakdown of filaments over aggregates in the GAN cells, which provided further evidence for the idea that calpain proteins were involved in this rapid, stress-induced degradation mechanism. The mechanisms by which calpain-2 associates with the perinuclear vimentin aggregates in GAN cells remain to be defined. We hypothesized that hypotonic stress-induced phosphorylation of vimentin may play a role in the release of calpain-2 from the aggregates, thereby leading to increased vimentin cleavage within the cytoplasmic network.

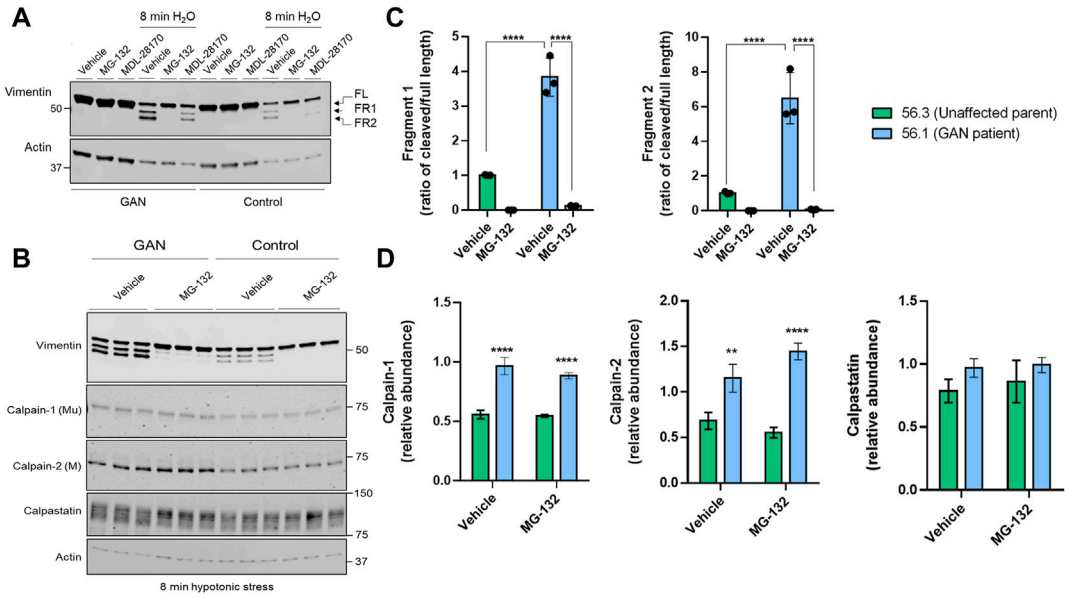

FIGURE 3
Vimentin cleavage is blocked by inhibitors of the proteasome and calpains, which are elevated in GAN. **(A)** Immunoblotting for vimentin (top) and actin (bottom; loading control) in Triton X insoluble pellet fractions from untreated (lanes 1–3, 7–9) or water-exposed (lanes 4–6, 10–12) control 56.3 and GAN 56.1 fibroblasts in the absence or presence of the DMSO vehicle control, calpain inhibitor (MDL-28170), or calpain/proteasome inhibitor (MG-132). Note partial cleavage inhibition by MDL and near-complete inhibition by MG-132. **(B)** Immunoblotting for vimentin (top) and actin (bottom; loading control) in reduced Triton X insoluble fractions and for calpain-1 (middle top), calpain-2 (middle), and calpastatin (middle bottom) in reduced Triton X soluble fractions from GAN and control fibroblasts exposed to 8 min of hypotonic stress and treated with the DMSO vehicle control or MG-132. Shown are technical replicates from an individual experiment. The experiment was independently repeated at least 3 times. **(C)** Quantification of the relative fragment 1 (FR1) and fragment 2 (FR2) band intensities normalized to the full length vimentin band for each cell line (GAN 56.1 fibroblasts; control 56.3 fibroblasts) and treatment group (from panel B). ****$p < 0.0001$; two-way ANOVA. **(D)** Quantification of calpain-1, calpain-2, and calpastatin levels (from panel B). **$p < 0.01$; ****$p < 0.0001$; two-way ANOVA.

Site-specific and time-dependent dephosphorylation in response to hypotonic stress regulates vimentin solubility. Phosphorylation sites on vimentin isolated from untreated or hypotonic stress-exposed GAN fibroblasts were mapped by mass spectrometry analysis (Figure 5A). Somewhat surprisingly, we did not observe a significant increase in vimentin phosphorylation at the sites identified in the head (S29, S39, S42, S56), rod (Y276), and tail (S409/412, T426, S430) domains. However, we noted a highly time-dependent decrease in S409/412 phosphorylation that was statistically significant and unique among the sites that were identified in the analysis (Figure 5A). Moreover, predictive analysis of calpain cleavage sites on vimentin using DeepCalpain identified cleavage within peptide 411–426, which contains the pSer412 site and the 418–419 predicted calpain-targeted junction (Figure 5B). Based on AlphaFold analysis, this serine residue marks the end of the coiled-coil rod domain (Figure 5C), suggesting that it likely has an important role in filament dynamics. To test that, we made phospho-mimic (S409D, S412D) and phospho-deficient (S409A, S412A) mutants and determined how they affected vimentin cleavage. Using BHK-21 fibroblasts, we over-expressed WT and mutant vimentin for 24 h and induced cleavage by water treatment. Consistent with the proteomic analysis, we observed increased cleavage in the phospho-deficient S412A mutant (Figure 5D), albeit not statistically significant (Figure 5E). However, in the case of over-expressed vimentin, the fragments were detected primarily in the soluble fraction (Figure 5D) and solubility was significantly decreased in the S412D phospho-mimic mutant (Figure 5F). In agreement with the reduced solubility, the S412D mutant exhibited abnormal filament structure with evidence of bundling, whereas S412A displayed bundles and normal filaments (Figure 5G). Of note, there were no changes in filament solubility or organization when Ser-409 was similarly mutated (not shown). Combined, these data demonstrated that Ser-412 is an important site for vimentin filament assembly and filament regulation during hypotonic stress exposure.

Discussion

In this study, we demonstrated that hypotonic stress exposure promoted rapid vimentin proteolysis and IF network breakdown in GAN patient-derived and unaffected control

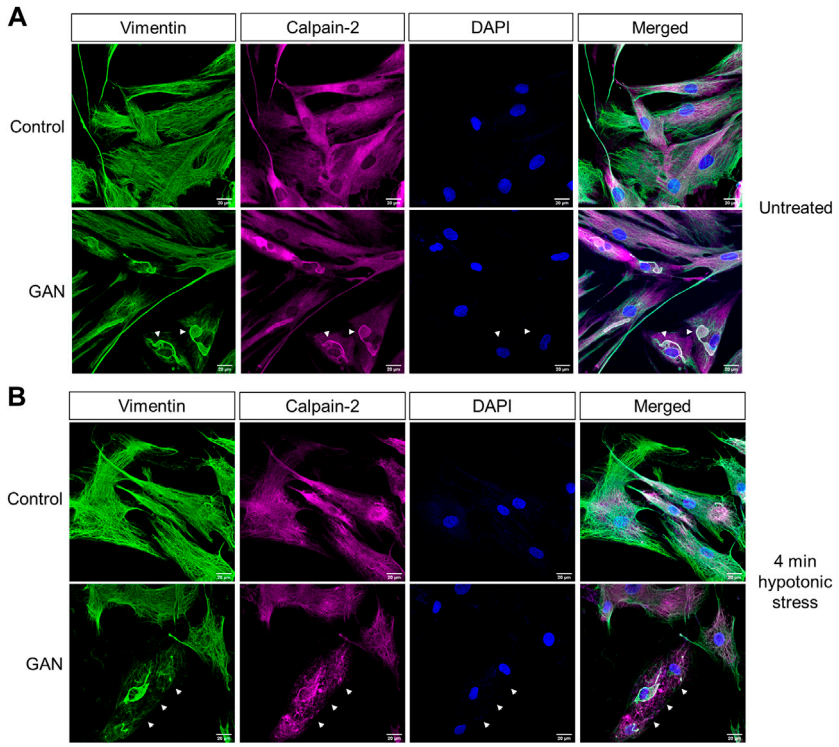

FIGURE 4
Calpain-2 colocalizes with perinuclear vimentin aggregates and undergoes cytoplasmic redistribution upon hypotonic stress exposure. **(A)** Calpain colocalizes with vimentin aggregates in untreated GAN fibroblasts. Immunofluorescence analysis of untreated control (56.3; top) and GAN (56.1; bottom) fibroblasts stained with vimentin (green), calpain-2 (magenta), and DAPI (blue); scale bar = 20 μm. Large perinuclear vimentin aggregates (green) colocalize with calpain-2 (magenta) in GAN patient cells (white arrowheads). **(B)** Calpain redistribution and vimentin network breakdown under hypotonic stress. Immunofluorescence analysis of control (56.3; top) and GAN (56.1; bottom) fibroblasts exposed to hypotonic stress for 4 min and stained with vimentin (green), calpain-2 (magenta), and DAPI (blue); scale bar = 20 μm. Calpain-2 (magenta) becomes more punctate and localized to vimentin filaments, indicating the selective loss of the vimentin filament network as compared to the relative preservation of vimentin aggregates (green) in GAN fibroblasts (white arrows).

fibroblasts. Surprisingly, we found that vimentin IFs in GAN fibroblasts were more sensitive to hypotonic stress-induced cleavage, suggesting that the presence of *KLHL16* mutations may be associated with increased IF fragmentation under stress. Based on pharmacological inhibition experiments, we concluded that this proteolytic pathway was a calpain- and proteasome-mediated process. Further studies are necessary to assess with a high degree of confidence the relative contribution of calpains and the ubiquitin-proteasome system (UPS) in GAN cells. However, there is existing evidence that calpains operate upstream of the UPS in desmin IF fragmentation that is thought to precede myofibril destruction (Aweida and Cohen, 2021). This process involves desmin phosphorylation, ubiquitination, and calpain cleavage prior to UPS-mediated degradation of myofibril-associated proteins (Aweida et al., 2018). Thus, calpain-mediated proteolysis in this context is considered a necessary step to 'loosen' the fibrillar structures and render them more accessible to further processing and degradation by the UPS (Aweida et al., 2018; Aweida and Cohen, 2021). This is also supported by evidence in muscular dystrophy caused by a loss-of-function mutation in the calpain-3 gene that results in impaired ubiquitination and proteasomal degradation of damaged proteins, leading to muscle weakness and atrophy (Kramerova et al., 2005). As vimentin and desmin IFs are known to undergo similar processing by calpains (Nelson and Traub, 1983b), we speculate that the coordinated actions of calpains and the UPS may also occur in GAN cells exposed hypotonic stress, but this remains to be tested in great detail.

The pure water-based hypotonic stress model we employed in the present study has been shown to lead to calpain-mediated fragmentation of vimentin IFs in response to calcium (Pan et al., 2019). This is consistent with previous studies showing that signaling events activated by elevated cytosolic calcium (due to influx or release from intracellular stores) cause rapid rearrangements of the cytoskeleton during cell swelling, in part by activation of calcium-dependent proteases (McCarty and O'Neil, 1992; Jakab et al., 2002). In the case of vimentin, the filaments were shown to be especially sensitive and

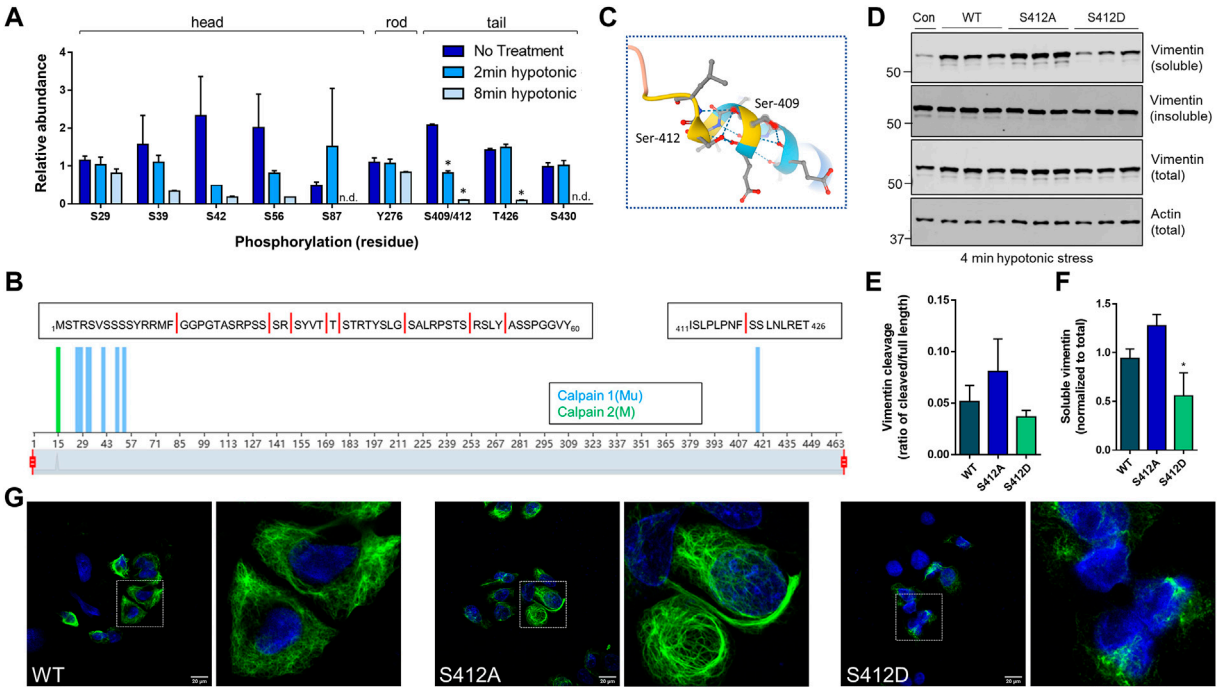

FIGURE 5
Site-specific and time-dependent dephosphorylation in response to hypotonic stress regulates vimentin solubility. **(A)** Mass spectrometry analysis for phosphorylation site changes on vimentin in GAN fibroblasts after 2 min and 8 min of hypotonic stress exposure. *$p < 0.001$; Multiple t-tests. **(B)** Predictive analysis of calpain cleavage sites on vimentin using the DeepCalpain tool. Peptide sequences span the N-terminal head domain (aa1-60), containing eight predicted cut sites (red lines) and C-terminal tail domain peptide (aa411-426) containing a single predicted cut site. **(C)** Model of vimentin rod/tail junction (AlphaFold) with the localization of Ser-409/412. **(D)** Immunoblotting for vimentin (top, middle) and actin (bottom; loading control) in Triton X soluble (top), Triton X insoluble (middle top), and total cell (middle bottom, bottom) lysates from BHK-21 cells transfected with WT, S412A, and S412D constructs and exposed to hypotonic stress for 4 min. **(E,F)** Quantification of vimentin cleavage **(E)** and solubility **(F)** in WT and mutant vimentin. *$p < 0.05$; one-way ANOVA. **(G)** Immunofluorescence analysis of SW13 Vim$^-$ cells transfected with WT vimentin (left) and vimentin mutants S412A (middle) and S412D (right) and stained with vimentin (green) and DAPI (blue) following a 24-h transfection period; scale bar = 20 μm. White squares indicate magnified areas.

responsive to hypotonic stress-induced calcium release from the ER that was triggered by inositol-3 phosphate (IP3) (Pan et al., 2019). Inhibition or sequestering of IP3 receptors, cytosolic calcium, and calpains decreased calpain activity in response to hypotonic stress, providing evidence for the involvement of this pathway in stress-induced vimentin proteolysis (Pan et al., 2019).

Whether proteolytic vimentin fragments have distinct functions and whether they regulate acute and chronic cellular stress response and recovery remains to be elucidated. We speculate that any potential biological function of the fragments will likely be determined by their stability in the cell. Many calpain-generated fragments are short-lived because they are substrates for the N-end rule pathway, a ubiquitin-proteasome dependent system that recognizes destabilizing N-terminal residues (Arg, Lys, His, Leu, Trp, Phe, Tyr, and Ile), which are directly recognized by N-recognins (Piatkov et al., 2014). However, most of the predicted calpain cut sites on vimentin expose an N-terminal residue on the resulting fragment that would be highly stabilizing (half-life >30 h) (Bachmair et al., 1986); including the putative head (N-terminal Ser, Ala, Gly), and tail (N-terminal Ser) domain fragments (Figure 5B). Based on such observations, we hypothesize that the vimentin fragments will be long-lived and may exert a significant impact on cellular function. This will be tested in future work, particularly in the context of GAN disease-relevant cell types harboring abnormal IF aggregates, specifically neurons and astrocytes. In many pathological states, including neurodegeneration and traumatic brain injury, astrocytes may undergo a response, known as *"clasmatodendrosis"*, morphologically reflected in IF network breakdown of their cytoskeletal proteins, including GFAP and vimentin (Balaban et al., 2021). Clasmatodendrosis (from Greek *klasma*, fragment, + *dendron*, tree, + *osis*, condition), is characterized by prominent swelling of the astrocyte cell body, together with pronounced beading and fragmentation of astrocyte cytoplasmic processes, readily visualized by GFAP and vimentin staining (Tomimoto et al., 1997; Early et al., 2020). It will be an important consideration to determine how stress-induced vimentin and GFAP cleavage and IF network fragmentation transpire mechanistically and how this response

affects astrocyte function. Such insights may help resolve the issue of whether clasmatodendrosis represents postmortem autolysis, or, instead, *in vivo* ongoing pathologic remodeling of astrocytes (Escartin et al., 2021).

Our imaging analysis showed striking colocalization between perinuclear vimentin aggregates and calpain-2, which had significantly increased expression in the GAN patient fibroblasts. While the reason for the increased calpain expression in GAN fibroblasts remains to be investigated, it is possible that association with vimentin aggregates promotes calpain stability. Active calpain-2 has been localized to protein aggregates associated with other neurodegenerative diseases, such as hyper-phosphorylated Tau protein (Adamec et al., 2002). In that regard, GAN may share similar mechanisms to other neurodegenerative disorders. In Alzheimer's disease (AD), calpain proteases may be involved in the proteolysis of amyloid precursor protein (APP), which is involved in the formation of amyloid plaques (Metwally et al., 2021). Interestingly, AD mice treated with calpastatin to inhibit calpain activity exhibited improved cognitive function and synaptic transmission (Rao et al., 2014). Additionally, treatment with calpastatin or other calpain inhibitors mitigated dopaminergic neuron loss in mice with Parkinson's disease (PD) (Crocker et al., 2003). Furthermore, calpain-mediated cleavage of TDP-43 in motor neurons contributes to the aggregates observed in Amyotrophic lateral sclerosis (ALS) (Yamashita et al., 2012). Increased levels of activated calpains have been detected in postmortem tissue from the prefrontal cortex and caudate nucleus of patients with AD and Huntington's disease (HD) respectively (Saito et al., 1993; Gafni and Ellerby, 2002). Since calpain-mediated cleavage is implicated in multiple neurodegenerative diseases that are characterized by abnormal protein aggregation, it is plausible that calpain proteases may also contribute to the pathologic IF accumulations observed in GAN through cleavage of IF proteins. This mechanism warrants investigation in future studies to determine if there are overlapping cellular mechanisms between GAN and other neurodegenerative diseases known to exhibit elevated calpain activity (Metwally et al., 2021).

Colocalization between vimentin and calpain-2 was significantly altered by hypotonic stress exposure, where selective breakdown of cytoplasmic IF networks with relative sparing of IF aggregates occurred rapidly in the patient cells and coincided with cytoplasmic redistribution of calpain-2. If, similar to the reported calpain-2/Tau interactions, calpain-2 associates with hyper-phosphorylated vimentin within the perinuclear aggregate, then decreased phosphorylation of vimentin upon stress induction may sever that interaction. Post-translational modifications (PTMs), particularly phosphorylation, are known to regulate IF functions and properties, including mediating IF stress responses (Snider and Omary, 2014). PTMs can serve as a precursor to additional responses, such as reorganization or degradation during or following a stress event. Our mass spectrometry-based proteomics indicated that phosphorylation at Ser-412 on vimentin is involved in this hypotonic stress response. This residue has not been well-characterized in the literature, although some groups have observed phosphorylation at residue S412 under physiological conditions (Snider and Omary, 2014; Lois-Bermejo et al., 2022). Recently, it was shown that modifications to S412 may influence filament assembly or positioning of the tail domain (Lois-Bermejo et al., 2022). Under normal conditions, an antibody targeting the 411–423 epitope of vimentin readily detected filaments throughout the network, whereas another epitope localized to the 419–438 segment was less accessible except for areas with rarefied filaments due to a compacted formation of the tail (Lois-Bermejo et al., 2022). Interestingly, both epitopes were similarly accessible with a phospho-mimic S412 vimentin mutant, suggesting that the tail domain was in a more open formation as a result of the mutation (Lois-Bermejo et al., 2022). Those findings, along with our data, support the idea that Ser-412 regulates vimentin filament organization, solubility, and degradation. Future efforts will be dedicated to further probing the relationship between key regulatory PTMs sites and proteolytic fragmentation of vimentin in response to osmotic stress.

Astrocytes are key players in the maintenance of cell volume homeostasis in the brain since they oversee fluxes of ions, water, and osmolytes at their homeostatic concentrations (Mola et al., 2021). Astrocyte IFs, including vimentin, are critical structures for cellular stress responses because astrocytes are sensitive to stress exposure, including osmotic and mechanical stresses resulting from ischemia, trauma, and brain edema (Pekny and Lane, 2007; Hol and Pekny, 2015; Murphy et al., 2017). The responsive nature of these cells can result in a "*reactive*" astrocyte phenotype, which may be beneficial during acute stress, but detrimental with chronic and prolonged stress (Escartin et al., 2021). Reactive astrocytes are prominent in GAN and other neurodegenerative disorders. Additionally, GAN astrocytes exhibit striking GFAP aggregates that co-accumulate with vimentin. Currently, it is unclear how abnormal cytoplasmic IF aggregates affect GAN astrocyte function, nor is it clear how impaired astrocyte function contributes to the disease pathology observed in GAN. Further, it remains unknown how GAN astrocyte IF aggregates and IF cytoplasmic networks respond under conditions of cellular stress. Our work described herein can serve as a springboard to address these questions in future studies.

Methods

Antibodies

The following primary antibodies and concentrations were utilized: rabbit anti-Vimentin (Cell Signaling Technology, D21H3, WB 1:1,000, IF 1:200), mouse anti-Vimentin

(Invitrogen, V9, WB 1:1,000–1:2,500, IF 1:100), mouse anti-Actin (Thermo Fisher Scientific, ACTN05, WB 1:1,000), mouse anti-Actin (Santa Cruz, SPM161, WB 1:1,000), rabbit anti-Calpastatin (Cell Signaling Technology, WB 1:1,000), rabbit anti-Calpain 1 (Cell Signaling Technology, large subunit Mu-type, WB 1:1,000), rabbit anti-Calpain 2 (Cell Signaling Technology, large subunit M-type, WB 1:1,000), and rabbit anti-Calpain 2 (Cell Signaling Technology, large subunit M-type, E3M6E, IF 1:200). The following secondary antibodies and concentrations were utilized: IRDye 800CW goat anti-rabbit IgG (LI-COR, WB 1:5,000), IRDye 680RD donkey anti-mouse IgG (LI-COR, WB 1:5,000), and Alexa 488- and Alexa 568-conjugated goat anti-mouse and anti-rabbit antibodies (Invitrogen, IF 1:500).

Cell lines

The following cell lines were used: control human skin fibroblasts from American Tissue Type Collection (ATCC), GAN patient fibroblast lines GAO1B and B16.64, paired GAN patient (56.1) and unaffected parent control (56.3) fibroblast lines, BHK-21 fibroblasts, and SW13 vimentin negative (Vim^-) cells as specified in the legends. The GAN cells (provided by Dr. Steven Gray) were thawed initially in DMEM (Gibco) in 20% fetal bovine serum (FBS; GenClone, Lot: P093156) and 1% penicillin/streptomycin (Thermo Fisher Scientific) and passaged every 3–4 days with 0.05% Trypsin-EDTA (Gibco), and after a few passages, the cells were maintained in 10% FBS media. SW13 Vim^- cells and BHK-21 cells were thawed and maintained in DMEM (Gibco) in 10% FBS (GenClone, Lot: P093156) and 1% penicillin/streptomycin (Thermo Fisher Scientific) and passaged every 3–4 days with 0.25% Trypsin-EDTA (Gibco).

Hypotonic stress experiments

GAN patient-derived and normal control fibroblasts grown to 70–80% confluence were exposed to hypotonic stress using pure water exposure, using a protocol that was detailed by Pan et al. previously (Pan et al., 2019). For biochemical hypotonic stress experiments, the cells were plated on 6-well plates and treated with sterile molecular grade water (Corning). Following aspiration of media, the cells were treated 3ml/well of water and incubated in a 37°C incubator for the designated timepoint (i.e., 0 min, 30 sec, 1 min, 2 min, 4 min, or 8 min). After treatment, the water was aspirated and Triton X-100 buffer (1% Triton X-100, 0.5 M EDTA, PBS, ddH_2O; pH 7.4) with 1X cOmplete™ Protease Inhibitor Cocktail and PhosSTOP™ Phosphatase Inhibitor Cocktail tablets (Roche; followed manufacturer directions) was added directly to each well. With the plate on ice, the cells were scraped from the wells and collected into Eppendorf tubes. At this stage, total cell lysate (TCL) samples were prepared by transferring 20% of the sample to a new tube and adding an equal volume of 2X Novex™ Tris-Glycine SDS Sample Buffer (Thermo Fisher Scientific). The remaining samples were spun down in a tabletop centrifuge at 12,000 rpm at 4°C to separate the detergent-soluble and insoluble fractions. The supernatant of the samples was transferred to a new tube, and for the soluble fraction, a smaller volume was then aliquoted to a different tube with an equal volume of SDS sample buffer. The remaining pellet was resuspended in SDS sample buffer to make the insoluble fraction. In experiments where only TCL fractions were analyzed, the cells were directly lysed in SDS sample buffer. All samples with SDS sample buffer were heated at 95°C for 5 min and reduced with 5% 2-mercaptoethanol (Sigma) as needed.

Pharmacological inhibition of calpain proteins

MDL-28170 (Cell Signaling Technology): A 100 mM MDL-28170 stock solution was made by dissolving the entire vial (5 mg) in DMSO. GAN patient and control fibroblasts were plated on 6-well plates, then pre-treated for 1 h in a 37°C incubator with the inhibitor or the DMSO vehicle control; the final inhibitor concentration of 100 μM (based on IC_{50} value of 10 μM) was achieved by adding 500 μL of inhibitor solution to 2.5 ml media already in the wells. Following pre-treatment, cells were treated with either the inhibitor or the DMSO vehicle control both with and without sterile molecular grade water; the final inhibitor concentration of 100 μM was achieved by adding 3 ml/well of the inhibitor/water (hypotonic treatment) or inhibitor/media (no treatment) solutions. The cells were exposed to hypotonic stress for 8 min (+/− inhibitor) in a 37°C incubator, then harvested and separated into TCL, detergent-soluble, and detergent-insoluble fractions as described above. *MG-132 (Cell Signaling Technology):* A 10 mM MG-132 stock solution was made by dissolving the entire vial (1 mg) in DMSO. GAN patient and control fibroblasts were plated on 6-well plates, then pre-treated for 1 h in a 37°C incubator with the inhibitor or the DMSO vehicle control; the final inhibitor concentration of 10 μM (based on IC_{50} value of 1.25 μM) was achieved by adding 500 μL of inhibitor solution to 2.5 ml media already in the wells. Following pre-treatment, cells were treated with either the inhibitor or the DMSO vehicle control both with and without sterile molecular grade water; the final inhibitor concentration of 10 μM was achieved by adding 3 ml/well of the inhibitor/water (hypotonic treatment) or inhibitor/media (no treatment) solutions. The cells were exposed to hypotonic stress for 8 min (+/− inhibitor) in a 37°C incubator, then harvested and separated into TCL,

detergent-soluble, and detergent-insoluble fractions as described above.

Site-directed mutagenesis and transfection of vimentin mutants

Mutagenesis of vimentin (pCMV6-XL5 vector; Origene) was conducted with the QuikChange II Site-Directed Mutagenesis Kit (Aligent Technologies) to generate the following point mutations: S409A, S409D, S409E, S412A, S412D, and S412E. Sanger sequencing for the entire vimentin coding sequence was completed to verify that the point mutations were present in the sequence without off-target changes. For transfection experiments for immunofluorescence imaging, SW13 Vim^- cells were seeded onto 4-well chamber slides and transfected with vimentin wild-type and mutant plasmids along with lipofectamine 2000 that was utilized in accordance with product instructions (Thermo Fisher Scientific). Media was changed 6 h after transfection, and cells were fixed at the 24-h timepoint (see below for details on immunofluorescence staining procedures). For biochemical transfection and hypotonic stress experiments, BHK-21 cells were plated on 6-well plates and transfected with vimentin wild-type and mutant plasmids plus lipofectamine 2000. Media was changed 6 h after transfection, and cells were treated with sterile molecular grade water at the 24-h timepoint. The cells were treated with hypotonic stress for 4 min in a 37°C incubator, then harvested and separated into TCL, detergent-soluble, and detergent-insoluble fractions as described above.

Preparation of protein lysates and immunoblotting

For immunoblotting, samples were separated on 10% or 4–20% gradient Novex™ WedgeWell™ Tris-Glycine gels (Thermo Fisher Scientific) for 40 min at 225V and transferred at 40V overnight at 4°C onto nitrocellulose membranes. Gels were stained with Coomassie following each transfer to verify normalization. The membranes were blocked in 5% non-fat milk (NFM) dissolved into 0.1% tween 20/PBS (PBST) at room temperature for 30 min. The membranes were incubated in primary antibodies diluted in 5% NFM/PBST at room temperature for 1 h or at 4°C overnight (see concentrations above), then washed 3x with PBST for 5 min each. The membranes were incubated with secondary antibodies diluted in 5% NFM/PBST at room temperature for 1 h (see concentrations above), washed 3x with PBST and 1x with PBS for 5 min each, then scanned with a LI-COR Odyssey CLx machine. Protein lysates were normalized by either method: staining gel with Coomassie before running the western blots (densitometry conducted with Adobe Photoshop), or blotting for pan-actin and normalizing the bands of interest to the pan-actin band intensity (densitometry conducted with Image Studio version 5.2).

Immunofluorescence, imaging, and analysis

Control and GAN cells were grown to 50–60% confluence, exposed to hypotonic stress, fixed in methanol at -20°C for 15 min, washed 2–3x with PBS for 5 min each, and blocked in Buffer B (2.5% Bovine Serum Albumin (Sigma), 2% normal goat serum (Gibco), PBS) at room temperature for 1 h. Cells were incubated with primary antibodies (see concentrations above) at room temperature for 2 h, followed by 3x 5-min PBS washes, then incubated with Alexa Fluor-conjugated secondary antibodies (see concentrations above) at room temperature for 1 h and washed 3x with PBS for 5 min each. Finally, cells were incubated with DAPI (Invitrogen), washed 3x with PBS for 5 min each, and mounted in Fluoromount-G (SouthernBiotech) overnight. Cells were imaged on a Zeiss 880 confocal laser scanning microscope using a Plan-Neofluar 40x/1.3 oil WD0.21objective.

Mass spectrometry

Sample preparation

GAN patient fibroblasts were plated on 10 cm plates, then treated with 10ml/plate sterile molecular grade water in a 37°C incubator at designated timepoints (0 min, 2 min, and 8 min). After treatment, the water was aspirated and Triton X-100 buffer (see above for details) was added directly to each plate. With the plate on ice, the cells were scraped from the wells and collected into Eppendorf tubes, spun in a tabletop centrifuge at 12,000 rpm at 4°C, then the supernatant of the samples was transferred to a new tube. High salt buffer (KCL, NaCl, Tris-HCl, 0.5M EDTA, 0.5% Triton X-100, ddH_2O; pH 7.6) with phosphatase (Roche) and protease (Roche) inhibitors was added to the remaining pellets, the samples were thoroughly dounced, spun in a tabletop centrifuge at 12,000 rpm at 4°C, then the sample supernatant was transferred to a new tube. 1x PBS/EDTA 5 mM was added to the remaining pellets, which were vortexed and spun at 12,000 rpm at 4°C. The PBS wash was discarded and the remaining pellets were resuspended in SDS sample buffer to make insoluble fractions, which were then heated at 95°C for 5 min. Insoluble fraction samples were loaded in a 4–20% gradient gel and run for about 40 min at 225V, then the gel was stained with GelCode™ Blue Stain for 1 h at room temperature and de-stained overnight in DDI H_2O. The gel bands of interest were excised for mass spectrometry analysis, and the excised bands were reduced, alkylated, and digested overnight at 37°C with trypsin. The extracted peptides were desalted using C18 ZipTips.

LC/MS/MS analysis and data analysis

The samples were analyzed in duplicate on an Easy-nLC™ 1200-QExactive HF system (Thermo Fisher Scientific) as previously described (Battaglia et al., 2019), and the raw data was analyzed in Proteome Discoverer v2.5 (Thermo Fisher Scientific). The data were searched against the Uniprot human database appended with a database of common contaminants, and tryptic peptides were identified using the following parameters: precursor mass tolerance was set to 10 ppm, fragment mass tolerance was set to 20 ppm, and up to two missed cleavage sites were allowed. The variable modifications were set to phosphorylation of Ser, Thr, and Tyr, and oxidation of methionine. The ptmRS node was used to localize phosphorylation sites. The false discovery rate (FDR) was set to 1% and used to filter all data.

Statistics

Image Studio version 5.2 (LI-COR) was used to perform densitometry on immunoblots, and Adobe Photoshop was used for densitometry on gels stained with Coomassie. To quantify vimentin cleavage, the relative intensities of the cleaved vimentin fragment bands were measured *via* densitometry, then normalized to the intensity of the full length vimentin band present in the samples. To quantify changes in solubility, the relative intensities of the full length vimentin bands in the detergent-soluble and insoluble fractions were measured *via* densitometry, then normalized to the intensity of the full length vimentin band in the total cell lysates. The expression levels of calpain-1, calpain-2, and calpastatin were measured *via* densitometry. The graphical data were generated using the GraphPad Prism software and analyzed using multiple T-tests (mass-spectrometry data; Figure 5A), one-way ANOVA (quantification of vimentin solubility and cleavage; Figures 5E,F), or two-way ANOVA (quantification of vimentin fragments and calpain-1, calpain-2, and calpastatin levels; Figures 3C,D) as noted in the Figure legends.

Data availability statement

The mass spectrometry proteomics data has been deposited to the ProteomeXchange Consortium via the PRIDE (Perez-Riverol Y, 2022) partner repository with the dataset identifier PXD037452.

Author contributions

CLP: Conceptualization, Data curation, Formal analysis, Funding acquisition, Validation, Investigation, Methodology, Writing—original draft, Writing—review and editing DF: Data curation, Formal analysis, Investigation, Methodology, Writing—review and editing LEH: Data curation, Formal analysis, Methodology, Writing—review and editing DA: Resources, Funding acquisition, Methodology, Writing—review and editing NTS: Conceptualization, Resources, Data curation, Formal analysis, Supervision, Funding acquisition, Validation, Investigation, Visualization, Methodology, Writing—original draft, Project administration, Writing—review and editing.

Funding

The work was supported by NIH grants: DK110355, NS121578, GM122741 (NIGMS Molecular Medicine T32), and Hannah's Hope Fund. This research is based in part upon work conducted using the UNC Proteomics Core Facility, which is supported in part by NCI Center Core Support Grant (2P30CA016086-45) to the UNC Lineberger Comprehensive Cancer Center.

Acknowledgments

We thank Jerald Whitley, Jr. for his technical assistance.

Conflict of interest

The authors declare that the research was conducted in the absence of any commercial or financial relationships that could be construed as a potential conflict of interest.

Publisher's note

References

Adamec, E., Mohan, P., Vonsattel, J. P., and Nixon, R. A. (2002). Calpain activation in neurodegenerative diseases: Confocal immunofluorescence study with antibodies specifically recognizing the active form of calpain 2. *Acta Neuropathol.* 104, 92–104. doi:10.1007/s00401-002-0528-6

Asbury, A., Gale, M., Cox, S., Baringer, J., and Berg, B. (1972). Giant axonal neuropathy—A unique case with segmental neurofilamentous masses. *Acta Neuropathol.* 20, 237–247. doi:10.1007/BF00686905

Aweida, D., and Cohen, S. (2021). Breakdown of filamentous myofibrils by the UPS–step by step. *Biomolecules* 11, 110. doi:10.3390/biom11010110

Aweida, D., Rudesky, I., Volodin, A., Shimko, E., and Cohen, S. (2018). GSK3-β promotes calpain-1–mediated desmin filament depolymerization and myofibril loss in atrophy. *J. Cell Biol.* 217, 3698–3714. doi:10.1083/jcb.201802018

Bachmair, A., Finley, D., and Varshavsky, A. (1986). *In vivo* half-life of a protein is a function of its amino-terminal residue. *science* 234, 179–186. doi:10.1126/science.3018930

Balaban, D., Miyawaki, E. K., Bhattacharyya, S., and Torre, M. (2021). The phenomenon of clasmatodendrosis. *Heliyon* 7, e07605. doi:10.1016/j.heliyon.2021.e07605

Battaglia, R. A., Beltran, A. S., Delic, S., Dumitru, R., Robinson, J. A., Kabiraj, P., et al. (2019). Site-specific phosphorylation and caspase cleavage of GFAP are new markers of Alexander disease severity. *Elife* 8, e47789. doi:10.7554/eLife.47789

Bharucha-Goebel, D. X., Norato, G., Saade, D., Paredes, E., Biancavilla, V., Donkervoort, S., et al. (2021). Giant axonal neuropathy: Cross sectional analysis of a large natural history cohort. *Brain.* 144, 3239–3250. doi:10.1093/brain/awab179

Bomont, P., Cavalier, L., Blondeau, F., Ben Hamida, C., Belal, S., Tazir, M., et al. (2000). The gene encoding gigaxonin, a new member of the cytoskeletal BTB/kelch repeat family, is mutated in giant axonal neuropathy. *Nat. Genet.* 26, 370–374. doi:10.1038/81701

Bourque, C. W. (2008). Central mechanisms of osmosensation and systemic osmoregulation. *Nat. Rev. Neurosci.* 9, 519–531. doi:10.1038/nrn2400

Coulombe, P. A., and Wong, P. (2004). Cytoplasmic intermediate filaments revealed as dynamic and multipurpose scaffolds. *Nat. Cell Biol.* 6, 699–706. doi:10.1038/ncb0804-699

Crocker, S. J., Smith, P. D., Jackson-Lewis, V., Lamba, W. R., Hayley, S. P., Grimm, E., et al. (2003). Inhibition of calpains prevents neuronal and behavioral deficits in an MPTP mouse model of Parkinson's disease. *J. Neurosci.* 23, 4081–4091. doi:10.1523/jneurosci.23-10-04081.2003

Davis, M. A., Fairgrieve, M. R., Den Hartigh, A., Yakovenko, O., Duvvuri, B., Lood, C., et al. (2019). Calpain drives pyroptotic vimentin cleavage, intermediate filament loss, and cell rupture that mediates immunostimulation. *Proc. Natl. Acad. Sci. U. S. A.* 116, 5061–5070. doi:10.1073/pnas.1818598116

Didonna, A., and Opal, P. (2019). The role of neurofilament aggregation in neurodegeneration: Lessons from rare inherited neurological disorders. *Mol. Neurodegener.* 14, 19–10. doi:10.1186/s13024-019-0318-4

Dourdin, N., Balcerzak, D., Brustis, J. J., Poussard, S., Cottin, P., and Ducastaing, A. (1999). Potential m-calpain substrates during myoblast fusion. *Exp. Cell Res.* 246, 433–442. doi:10.1006/excr.1998.4325

Dutour-Provenzano, G., and Etienne-Manneville, S. (2021). Intermediate filaments. *Curr. Biol.* 31, R522–R529. doi:10.1016/j.cub.2021.04.011

Early, A. N., Gorman, A. A., Van Eldik, L. J., Bachstetter, A. D., and Morganti, J. M. (2020). Effects of advanced age upon astrocyte-specific responses to acute traumatic brain injury in mice. *J. Neuroinflammation* 17, 115–116. doi:10.1186/s12974-020-01800-w

Escartin, C., Galea, E., Lakatos, A., O'Callaghan, J. P., Petzold, G. C., Serrano-Pozo, A., et al. (2021). Reactive astrocyte nomenclature, definitions, and future directions. *Nat. Neurosci.* 24, 312–325. doi:10.1038/s41593-020-00783-4

Etienne-Manneville, S. (2018). Cytoplasmic intermediate filaments in cell biology. *Annu. Rev. Cell Dev. Biol.* 34, 1–28. doi:10.1146/annurev-cellbio-100617-062534

Gafni, J., and Ellerby, L. M. (2002). Calpain activation in Huntington's disease. *J. Neurosci.* 22, 4842–4849. doi:10.1523/jneurosci.22-12-04842.2002

Hol, E. M., and Pekny, M. (2015). Glial fibrillary acidic protein (GFAP) and the astrocyte intermediate filament system in diseases of the central nervous system. *Curr. Opin. Cell Biol.* 32, 121–130. doi:10.1016/j.ceb.2015.02.004

Jakab, M., Fürst, J., Gschwentner, M., Bottà, G., Garavaglia, M.-L., Bazzini, C., et al. (2002). Mechanisms sensing and modulating signals arising from cell swelling. *Cell. Physiol. biochem.* 12, 235–258. doi:10.1159/000067895

Johnson-Kerner, B. L., Roth, L., Greene, J. P., Wichterle, H., and Sproule, D. M. (2014). Giant axonal neuropathy: An updated perspective on its pathology and pathogenesis. *Muscle Nerve* 50, 467–476. doi:10.1002/mus.24321

Kedia, N., Arhzaouy, K., Pittman, S. K., Sun, Y., Batchelor, M., Weihl, C. C., et al. (2019). Desmin forms toxic, seeding-competent amyloid aggregates that persist in muscle fibers. *Proc. Natl. Acad. Sci. U. S. A.* 116, 16835–16840. doi:10.1073/pnas.1908263116

Kramerova, I., Kudryashova, E., Venkatraman, G., and Spencer, M. J. (2005). Calpain 3 participates in sarcomere remodeling by acting upstream of the ubiquitin–proteasome pathway. *Hum. Mol. Genet.* 14, 2125–2134. doi:10.1093/hmg/ddi217

Ku, N. O., Strnad, P., Zhong, B. H., Tao, G. Z., and Omary, M. B. (2007). Keratins let liver live: Mutations predispose to liver disease and crosslinking generates mallory-denk bodies. *Hepatology* 46, 1639–1649. doi:10.1002/hep.21976

Leung, C. L., Pang, Y., Shu, C., Goryunov, D., and Liem, R. K. (2007). Alterations in lipid metabolism gene expression and abnormal lipid accumulation in fibroblast explants from giant axonal neuropathy patients. *BMC Genet.* 8, 6. doi:10.1186/1471-2156-8-6

Li, J., Gao, W., Zhang, Y., Cheng, F., Eriksson, J. E., Etienne-Manneville, S., et al. (2019). Engagement of vimentin intermediate filaments in hypotonic stress. *J. Cell. Biochem.* 120, 13168–13176. doi:10.1002/jcb.28591

Lois-Bermejo, I., González-Jiménez, P., Duarte, S., Pajares, M. A., and Pérez-Sala, D. (2022). Vimentin tail segments are differentially exposed at distinct cellular locations and in response to stress. *Front. Cell Dev. Biol.* 10, 908263. doi:10.3389/fcell.2022.908263

Lowery, J., Kuczmarski, E. R., Herrmann, H., and Goldman, R. D. (2015). Intermediate filaments play a pivotal role in regulating cell architecture and function. *J. Biol. Chem.* 290, 17145–17153. doi:10.1074/jbc.R115.640359

Mahammad, S., Murthy, S. N., Didonna, A., Grin, B., Israeli, E., Perrot, R., et al. (2013). Giant axonal neuropathy-associated gigaxonin mutations impair intermediate filament protein degradation. *J. Clin. Invest.* 123, 1964–1975. doi:10.1172/JCI66387

McCarty, N. A., and O'Neil, R. G. (1992). Calcium signaling in cell volume regulation. *Physiol. Rev.* 72, 1037–1061. doi:10.1152/physrev.1992.72.4.1037

Metwally, E., Zhao, G., and Zhang, Y. Q. (2021). The calcium-dependent protease calpain in neuronal remodeling and neurodegeneration. *Trends Neurosci.* 44, 741–752. doi:10.1016/j.tins.2021.07.003

Mohri, I., Taniike, M., Yoshikawa, H., Higashiyama, M., Itami, S., and Okada, S. (1998). A case of giant axonal neuropathy showing focal aggregation and hypophosphorylation of intermediate filaments. *Brain Dev.* 20, 594–597. doi:10.1016/s0387-7604(98)00056-4

Mola, M. G., Saracino, E., Formaggio, F., Amerotti, A. G., Barile, B., Posati, T., et al. (2021). Cell volume regulation mechanisms in differentiated astrocytes. *Cell. Physiol. biochem.* 55, 196–212. doi:10.33594/000000469

Murphy, T. R., Davila, D., Cuvelier, N., Young, L. R., Lauderdale, K., Binder, D. K., et al. (2017). Hippocampal and cortical pyramidal neurons swell in parallel with astrocytes during acute hypoosmolar stress. *Front. Cell. Neurosci.* 11, 275. doi:10.3389/fncel.2017.00275

Nalini, A., Gayathri, N., Yasha, T. C., Ravishankar, S., Urtizberea, A., Huehne, K., et al. (2008). Clinical, pathological and molecular findings in two siblings with giant axonal neuropathy (GAN): Report from India. *Eur. J. Med. Genet.* 51, 426–435. doi:10.1016/j.ejmg.2008.05.006

Nelson, W. J., and Traub, P. (1983). Proteolysis of vimentin and desmin by the Ca2+-activated proteinase specific for these intermediate filament proteins. *Mol. Cell. Biol.* 3, 1146–1156. doi:10.1128/mcb.3.6.1146

Nelson, W. J., and Traub, P. (1983). Proteolysis of vimentin and desmin by the Ca2+-activated proteinase specific for these intermediate filament proteins. *Mol. Cell. Biol.* 3, 1146–1156. doi:10.1128/mcb.3.6.1146

Pan, L., Zhang, P., Hu, F., Yan, R., He, M., Li, W., et al. (2019). Hypotonic stress induces fast, reversible degradation of the vimentin cytoskeleton via intracellular calcium release. *Adv. Sci.* 6, 1900865. doi:10.1002/advs.201900865

Pekny, M., and Lane, E. B. (2007). Intermediate filaments and stress. *Exp. Cell Res.* 313, 2244–2254. doi:10.1016/j.yexcr.2007.04.023

Perez-Riverol, Y., Bai, J., Bandla, C., Hewapathirana, S., García-Seisdedos, D., Kamatchinathan, S., et al. (2022). The PRIDE database resources in 2022: A Hub for mass spectrometry-based proteomics evidences. *Nucleic Acids Res* 50(D1): D543–D552.

Piatkov, K. I., Oh, J.-H., Liu, Y., and Varshavsky, A. (2014). Calpain-generated natural protein fragments as short-lived substrates of the N-end rule pathway. *Proc. Natl. Acad. Sci. U. S. A.* 111, E817–E826. doi:10.1073/pnas.1401639111

Rainer, P. P., Dong, P., Sorge, M., Fert-Bober, J., Holewinski, R. J., Wang, Y., et al. (2018). Desmin phosphorylation triggers preamyloid oligomers formation and myocyte dysfunction in acquired heart failure. *Circ. Res.* 122, e75–e83. doi:10.1161/CIRCRESAHA.117.312082

Rakoski, M. O., Brown, M. B., Fontana, R. J., Bonkovsky, H. L., Brunt, E. M., Goodman, Z. D., et al. (2011). Mallory–denk bodies are associated with outcomes

and histologic features in patients with chronic hepatitis C. *Clin. Gastroenterol. Hepatol.* 9, 902–909. doi:10.1016/j.cgh.2011.07.006

Rao, M. V., McBrayer, M. K., Campbell, J., Kumar, A., Hashim, A., Sershen, H., et al. (2014). Specific calpain inhibition by calpastatin prevents tauopathy and neurodegeneration and restores normal lifespan in tau P301L mice. *J. Neurosci.* 34, 9222–9234. doi:10.1523/JNEUROSCI.1132-14.2014

Robertson, J., Beaulieu, J.-M., Doroudchi, M. M., Durham, H. D., Julien, J.-P., and Mushynski, W. E. (2001). Apoptotic death of neurons exhibiting peripherin aggregates is mediated by the proinflammatory cytokine tumor necrosis factor-alpha. *J. Cell Biol.* 155, 217–226. doi:10.1083/jcb.200107058

Saito, K., Elce, J. S., Hamos, J. E., and Nixon, R. A. (1993). Widespread activation of calcium-activated neutral proteinase (calpain) in the brain in alzheimer disease: A potential molecular basis for neuronal degeneration. *Proc. Natl. Acad. Sci. U. S. A.* 90, 2628–2632. doi:10.1073/pnas.90.7.2628

Snider, N. T., and Omary, M. B. (2014). Post-translational modifications of intermediate filament proteins: Mechanisms and functions. *Nat. Rev. Mol. Cell Biol.* 15, 163–177. doi:10.1038/nrm3753

Sosunov, A. A., McKhann, G. M., and Goldman, J. E. (2017). The origin of Rosenthal fibers and their contributions to astrocyte pathology in Alexander disease. *Acta Neuropathol. Commun.* 5, 27–14. doi:10.1186/s40478-017-0425-9

Thomas, C., Love, S., Powell, H. C., Schultz, P., and Lampert, P. W. (1987). Giant axonal neuropathy: Correlation of clinical findings with postmortem neuropathology. *Ann. Neurol.* 22, 79–84. doi:10.1002/ana.410220118

Toivola, D., Strnad, P., Habtezion, A., and Omary, M. (2010). Intermediate filaments take the heat as stress proteins. *Trends Cell Biol.* 20, 79–91. doi:10.1016/j.tcb.2009.11.004

Tomimoto, H., Akiguchi, I., Wakita, H., Suenaga, T., Nakamura, S., and Kimura, J. (1997). Regressive changes of astroglia in white matter lesions in cerebrovascular disease and Alzheimer's disease patients. *Acta Neuropathol.* 94, 146–152. doi:10.1007/s004010050686

Viedma-Poyatos, Á., Pajares, M. A., and Pérez-Sala, D. (2020). Type III intermediate filaments as targets and effectors of electrophiles and oxidants. *Redox Biol.* 36, 101582. doi:10.1016/j.redox.2020.101582

Xiao, S., Tjostheim, S., Sanelli, T., McLean, J. R., Horne, P., Fan, Y., et al. (2008). An aggregate-inducing peripherin isoform generated through intron retention is upregulated in amyotrophic lateral sclerosis and associated with disease pathology. *J. Neurosci.* 28, 1833–1840. doi:10.1523/JNEUROSCI.3222-07.2008

Yamashita, T., Hideyama, T., Hachiga, K., Teramoto, S., Takano, J., Iwata, N., et al. (2012). A role for calpain-dependent cleavage of TDP-43 in amyotrophic lateral sclerosis pathology. *Nat. Commun.* 3, 1307–1313. doi:10.1038/ncomms2303

Yang, A.-W., Lin, N.-H., Yeh, T.-H., Snider, N., and Perng, M.-D. (2022). Effects of Alexander disease-associated mutations on the assembly and organization of GFAP intermediate filaments. *Mol. Biol. Cell* 33. 0013. doi:10.1091/mbc.e22-01-0013